Journal of Solid State Chemistry 182 (2009) 8–17

Contents lists available at ScienceDirect

Journal of Solid State Chemistry

journal homepage: www.elsevier.com/locate/jssc

Synthesis, crystal structure, and magnetic properties of two-dimensional divalent metal glutarate/dipyridylamine coordination polymers, with a single crystal-to-single crystal transformation in the copper derivative

Matthew R. Montney [a], Ronald M. Supkowski [b], Richard J. Staples [a], Robert L. LaDuca [a,*]

[a] Lyman Briggs College and Department of Chemistry, Michigan State University, East Lansing, MI 48825, USA
[b] Department of Chemistry and Physics, King's College, Wilkes-Barre, PA 18711, USA

ARTICLE INFO

Article history:
Received 22 May 2008
Received in revised form
8 September 2008
Accepted 21 September 2008
Available online 11 October 2008

Keywords:
Coordination polymer
Crystal structure
Dicarboxylate
SCSC
Antiferromagnetism
Ferromagnetism

ABSTRACT

Hydrothermal reaction of divalent metal chlorides with glutaric acid and 4,4′-dipyridylamine (dpa) has afforded an isostructural family of coordination polymers with formulation $[M(glu)(dpa)]_n$ (M = Co (**1**), Ni (**2**), Cu (**3**); glu = glutarate). Square pyramidal coordination is seen in **1**–**3**, with semi-ligation of a sixth donor to produce a "5+1" extended coordination sphere. Neighboring metal atoms are linked into 1D $[M(glu)]_n$ neutral chains through chelating/monodentate bridging glutarate moieties with a *syn–anti* binding mode, and semi-chelation of the pendant carboxylate oxygen. These chains further connect into 2D layers through dipodal dpa ligands. Neighboring layers stack into the pseudo 3D crystal structure of **1**–**3** through supramolecular hydrogen bonding between dpa amine units and the semi-chelated glutarate oxygen atoms. The variable temperature magnetic behavior of **1**–**3** was explored and modeled as infinite 1D Heisenberg chains. Notably, complex **3** undergoes a thermally induced single crystal-to-single crystal transformation between centric and acentric space groups, with a conformationally disordered unilayer structure at 293 K and an ordered bilayer structure at 173 K. All materials were further characterized via infrared spectroscopy and elemental and thermogravimetric analyses.

© 2008 Elsevier Inc. All rights reserved.

1. Introduction

Over the past decade intense investigation has focused on dicarboxylate metal-organic frameworks (MOFs) due to their capabilities in gas storage [1], shape-selective separations [2], ion-exchange [3], catalysis [4], non-linear optics [5], luminescence [6], and magnetism [7]. In these phases dianionic dicarboxylates act as tethering ligands to connect neighboring metal ions into a diverse range of structural motifs, hinged on the disposition of donor atoms and the ability of these ligands to adopt a wide variety of binding modes and to provide loci for structure-directing supramolecular hydrogen bonding interactions. They also allow the charge balance necessary to permit self-assembly of neutral MOFs without the incorporation of smaller anions that could inhibit formation of void spaces. The level of structural complexity in dicarboxylate MOFs can be enhanced through the introduction of neutral nitrogen-based tethering ligands such as 4,4′-bipyridine (4,4′-bpy), which can connect metal cations through its distal pyridyl nitrogen donor atoms into structurally intriguing solids with interesting physicochemical properties [8–10]. For example, the 2D layered phase $[Zn_4O(isophthalate)_3(4,4'\text{-bpy})]$ has potential use as a blue luminescent material [8], and the interpenetrated 3D material $[Zn(terephthalate)(4,4'\text{-bpy})_{0.5}]$ can chromatographically separate branched and linear hydrocarbons [9].

Compared with benzenedicarboxylate MOFs, organodiimine-scaffolded coordination polymers based on longer aliphatic α,ω-dicarboxylates have received less attention [10–14]. While the structural rigidity of benzenedicarboxylate subunits is advantageous for the construction of porous materials, flexible aliphatic dicarboxylates can provoke novel structural motifs due to their ability to access numerous energetically similar conformations. For instance, a few divalent metal adipate (adp) coordination polymers incorporating 4,4′-bpy or bpe have been reported, in all cases manifesting interpenetrated 3D networks with the well-known α-Po topology [10–12].

For some time we have been interested in the synthesis and characterization of coordination polymers containing the organodiimine 4,4′-dipyridylamine (dpa). Unlike 4,4′-bpy, dpa possesses a kinked disposition of its terminal nitrogen donor atoms as well as a hydrogen bonding locus at its center, allowing it to promote the formation of novel structural patterns via supramolecular as well as covalent interactions.

Combination of dpa and α,ω-dicarboxylic acids with appropriate metal precursors under hydrothermal conditions has resulted in the construction of extended solids with interesting

* Corresponding author.
E-mail address: laduca@msu.edu (R.L. LaDuca).

0022-4596/$ - see front matter © 2008 Elsevier Inc. All rights reserved.
doi:10.1016/j.jssc.2008.09.020

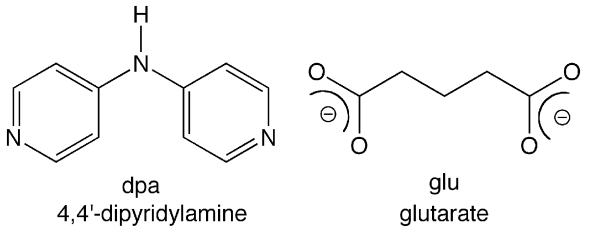

Scheme 1.

and diverse structural motifs [15–17]. For instance, [Co(succinate)(dpa)$_2$]$_n$ displays homochiral 1D helices linked together via dpa-mediated hydrogen bonding. {[Cu(succinate)(dpa)]·0.5H$_2$O}$_n$ adopts a rarely seen two-fold interpenetrated $CdSO_4$ lattice ($6^5 8$ topology), while {[Ni(dpa)$_2$(succinate)$_{0.5}$]Cl}$_n$ manifested a unique uniform 5-connected self-penetrated 6^{10} topology (*rld-z*) network [15]. The longer chain α,ω-dicarboxylate adipate allowed formation of [Co(adipate)(dpa)]$_n$, a material exhibiting a rather common two-fold interpenetrated primitive cubic 6-connected lattice. However, use of a divalent nickel precursor resulted in the crystallization of [Ni(adipate)(dpa)(H$_2$O)]$_n$, which is the first example of a triply interpenetrated PtS framework (binodal $4^2 8^4$ topology). Herein we report the first dpa-containing glutarate (glu, 1,5-pentanedicarboxylate, Scheme 1) coordination polymers with the hydrothermal synthesis and structural characterization of three related complexes, [M(glu)(dpa)]$_n$ (M = Co, **1**; M = Ni, **2**; M = Cu, **3**). Thermal and magnetic properties of these materials are also discussed, along with a curious thermally-induced ordered to disordered single crystal-to-single crystal (SCSC) transition in the case of compound **3**.

2. Experimental section

2.1. General considerations

$CoCl_2 \cdot 6H_2O$, $NiCl_2 \cdot 6H_2O$, $CuCl_2 \cdot 2H_2O$ (Fisher), and glutaric acid (Aldrich) were obtained commercially. 4,4′-dipyridylamine (dpa) was prepared via a published procedure [18]. Water was deionized above 3 MΩ in-house. Thermogravimetric analysis was performed on TA Instruments TGA 2050 thermogravimetric analyzer with a heating rate of 10 °C/min up to 900 °C under flowing N_2. Elemental Analysis was carried out using a Perkin–Elmer 2400 Series II CHNS/O Analyzer. IR spectra were recorded on a Mattson Galaxy FTIR Series 3000 using KBr pellets. Powder X-ray diffraction on ground samples of **1**–**3** for phase purity verification were obtained via Θ–2Θ scans performed on a Rigaku Rotaflex instrument. Variable temperature magnetic susceptibility data (2–300 K) was collected on a Quantum Design MPMS SQUID magnetometer at an applied field of 0.1 T. After each temperature change the sample was kept at the new temperature for 5 min before magnetization measurement to ensure thermal equilibrium. The susceptibility data was corrected for diamagnetism using Pascal's constants [19]. Differential scanning calorimetry on a sample of crystalline **3** was carried out using a TA Instruments DSC 2010 instrument.

2.2. Preparation of [Co(glu)(dpa)]$_n$ (*1*)

$CoCl_2 \cdot 6H_2O$ (88 mg, 0.37 mmol), dpa (127 mg, 0.73 mmol), and glutaric acid (49 mg, 0.37 mmol) were placed into 10 mL distilled H_2O in a 23 mL Teflon-lined Parr acid digestion bomb. The bomb was sealed and heated at 120 °C for 48 h, whereupon it was cooled slowly to 25 °C. Large single crystalline blocks of **1** (110 mg, 82% yield based on Co) were isolated after washing with distilled water, ethanol, and acetone and drying in air. Crystals of **1** display pleochroism, appearing brown, orange, or violet depending on their orientation with respect to a bright light source. Anal. Calc. for $C_{15}H_{15}CoN_3O_4$ **1**: C, 50.01; H, 4.20; N, 11.67%. Found: C, 49.50; H, 3.93; N, 11.43%. IR (KBr, cm^{-1}): 3450 w br (NH), 3292 w, 3074 w, 2971 m, 2925 s, 2858 m (CH), 1638 m, 1596 s (CO_2 asym), 1561 s, 1535 s, 1492 m, 1462 m, 1443 m, 1404 m, 1359 m (CO_2 sym), 1332 m, 1297 w, 1252 w, 1211 m, 1150 w, 1070 w, 1064 w, 1021 m, 910 w, 857 m, 819 m, 735 w, 677 w, 650 m, 620 w, 589 w, 532 m.

2.3. Preparation of [Ni(glu)(dpa)]$_n$ (*2*)

The procedure for **1** above was followed, using $NiCl_2 \cdot 6H_2O$ (88 mg, 0.37 mmol), dpa (127 mg, 0.73 mmol) and glutaric acid (49 mg, 0.37 mmol). For optimized yields, the best reaction temperature was determined to be 150 °C. Green blocks of **2** (72 mg, 54% yield based on Ni) were isolated after washing with distilled water, ethanol, and acetone and drying in air. Calc. for $C_{15}H_{15}NiN_3O_4$ **2**: C, 50.04; H, 4.20; N, 11.67%; Found: C, 49.84; H, 3.97; N, 11.55%. IR (KBr, cm^{-1}): 3450 w br (NH), 3292 w, 3074 w, 2971 m, 2921 s, 2848 m, 1638 m, 1577 s, 1557 s, 1538 s (CO_2 asym), 1508 m, 1492 m, 1466 m, 1443 m, 1404 m, 1359 m (CO_2 sym), 1332 m, 1295 w, 1252 w, 1213 m, 1152 w, 1070 w, 1064 w, 1021 m, 910 w, 861 m, 826 m, 734 w, 679 w, 658 m, 646 m, 631 w, 596 m, 543 m.

2.4. Preparation of [Cu(glu)(dpa)]$_n$ (*3*)

The procedure for **1** above was followed, using $CuCl_2 \cdot 2H_2O$ (63 mg, 0.37 mmol), dpa (127 mg, 0.73 mmol), and glutaric acid (49 mg, 0.37 mmol). Blue blocks of **3** (59 mg, 44% yield based on Cu) were isolated after washing with distilled water, ethanol, and acetone and drying in air. Calc. for $C_{15}H_{15}CuN_3O_4$ **3**: C, 49.38; H, 4.14; N, 11.52%. Found: C, 49.08; H, 3.99; N, 11.53%. IR (KBr, cm^{-1}): 2903 w br, 1632 w, 1580 s, 1542 s (CO_2 asym), 1523 s, 1487 s, 1455 m, 1440 m, 1416 m, 1388 m, 1351 s (CO_2 sym), 1327 m, 1299 m, 1274 w, 1251 w, 1207 s, 1160 w, 1067 w, 1057 m, 1042 w, 1024 s, 907 m, 857 w, 840 w, 819 s, 799 m, 730 w, 679 w, 663 w.

3. X-ray crystallography

A brown block of **1** (with dimensions 0.78 mm × 0.56 mm × 0.48 mm), a green block of **2** (0.42 mm × 0.20 mm × 0.18 mm), and a blue block of **3** (0.24 mm × 0.10 mm × 0.10 mm) were subjected to single crystal X-ray diffraction using a Bruker-AXS SMART 1k CCD instrument at 173 K. The X-ray diffraction experiment for the same single crystal of **3** was repeated at 293 K. Reflection data was acquired using graphite-monochromated Mo*K*α radiation ($\lambda = 0.71073$ Å). The data was integrated via SAINT [20]. Lorentz and polarization effect and empirical absorption corrections were applied with SADABS [21]. The structures were solved using direct methods and refined on F^2 using SHELXTL [22]. All non-hydrogen atoms were refined anisotropically. Hydrogen atoms bound to carbon atoms were placed in calculated positions and refined isotropically with a riding model. The hydrogen atoms bound to the central nitrogen of the dpa moieties in **1**–**3** were found via Fourier difference maps, then restrained at fixed positions and refined isotropically. Attempts to refine the crystal structure of **3** using the low temperature reflection data in the higher symmetry centrosymmetric space group *Pbcm* with a disordered glutarate conformation model resulted in unacceptably high wR_2 values (~0.52), with 355 systematic absence violations. Acceptable solution was possible

Table 1
Crystal and structure refinement data for **1**–**3**

Data	**1**	**2**
Empirical formula	$C_{15}H_{15}CoN_3O_4$	$C_{15}H_{15}N_3NiO_4$
Formula weight	360.23	360.01
Collection T (K)	173(2)	173(2)
λ (Å)	0.71073	0.71073
Crystal system	Orthorhombic	Orthorhombic
Space group	*Pbcn*	*Pbcn*
a (Å)	15.3995(12)	15.412(3)
b (Å)	8.2673(9)	8.2158(17)
c (Å)	23.476(3)	23.273(5)
V (Å^3)	2988.8(6)	2946.8(11)
Z	8	8
D_{calc} (g cm^{-3})	1.601	1.623
μ (mm^{-1})	1.173	1.341
Min/max trans.	0.868	0.821
hkl ranges	$-20\leqslant h\leqslant 20$	$-20\leqslant h\leqslant 19$
	$-11\leqslant k\leqslant 11$	$-10\leqslant k\leqslant 10$
	$-31\leqslant l\leqslant 31$	$-30\leqslant l\leqslant 31$
Total reflections	32906	33456
Unique reflections	3649	3649
R (int)	0.0193	0.0653
Parameters/restraints	212/0	211/1
R_1 (all data)	0.0268	0.0611
R_1 ($I>2\sigma(I)$)	0.0240	0.0394
wR_2 (all data)	0.0609	0.0880
wR_2 ($I>2\sigma(I)$)	0.0592	0.0795
Max/min residual (e$^-$/Å^3)	0.376/−0.257	0.489/−0.551
G.O.F.	1.058	1.063
Data	**3** (low temperature)	**3** (high temperature)
Empirical formula	$C_{30}H_{30}Cu_2N_6O_8$	$C_{15}H_{15}CuN_3O_4$
Formula weight	729.68	364.84
Collection T (K)	173(2)	293(2)
λ (Å)	0.71073	0.71073
Crystal system	Orthorhombic	Orthorhombic
Space group	*Pca2$_1$*	*Pbcn*
a (Å)	8.8730(10)	15.0653(17)
b (Å)	14.9974(16)	8.9015(10)
c (Å)	22.743(3)	22.769(3)
V (Å^3)	3026.5(6)	3053.4(6)
Z	4	8
D_{calc} (g cm^{-3})	1.601	1.587
μ (mm^{-1})	1.467	1.454
Min/max trans.	0.8299	0.8738
Hkl ranges	$-11\leqslant h\leqslant 11$,	$-19\leqslant h\leqslant 19$,
	$-19\leqslant k\leqslant 19$,	$-11\leqslant k\leqslant 11$,
	$-29\leqslant l\leqslant 29$	$-30\leqslant l\leqslant 29$
Total reflections	31 226	31 151
Unique reflections	6 970	3 624
R (int)	0.0292	0.0347
Parameters/restraints	422/3	238/1
R_1 (all data)	0.0260	0.0424
R_1 ($I>2\sigma(I)$)	0.0225	0.0295
wR_2 (all data)	0.0556	0.0773
wR_2 ($I>2\sigma(I)$)	0.0539	0.0719
Max/min residual (e$^-$/Å^3)	0.279/−0.258	0.329/−0.369
G.O.F.	1.040	1.046

[a] $R_1=\Sigma||F_o|-|F_c||/\Sigma|F_o|$. [b] $wR_2=\{\Sigma[w(F_o^2-F_c^2)^2]/\Sigma[wF_o^2]^2\}^{1/2}$.

only in *Pca2*$_1$ with racemic twinning taken into account. Conversely, the crystal structure of **3** could not be acceptably solved in an acentric orthorhombic space group using the high temperature reflection data. Relevant crystallographic data for **1**, **2**, and **3** (at both 173 and 293 K) are listed in Table 1.

4. Results and discussion

4.1. Synthesis and spectral characterization

The coordination polymers **1**–**3** were prepared as single phase crystalline products under hydrothermal conditions via combination of the appropriate metal chloride, 4,4′-dipyridylamine, and glutaric acid. The infrared spectra of **1**–**3** were fully consistent with their formulations. Features corresponding to pyridyl ring puckering mechanisms were evident in the region between 800 and 600 cm^{-1}. Sharp, medium intensity bands in the range of ~1600–~1200 cm^{-1} were ascribed to stretching modes of the pyridyl rings of the dpa moieties [23]. Asymmetric and symmetric C–O stretching modes of the glutarate carboxylate moieties were evidenced by very strong, slightly broadened bands at ~1580 and ~1350 cm^{-1}. The multiplicity of peaks in this region corroborates the presence of different binding modes present at each glutarate carboxylate terminus. Bands in the region of ~3400 cm^{-1} in all cases represent N–H stretching modes within the dpa ligands; their broadness is indicative of hydrogen bonding to carboxylate oxygen atoms (vide infra).

4.2. Structural description of [M(glu)(dpa)]$_n$ (M = Co, **1**; M = Ni, **2**)

As revealed by single-crystal X-ray diffraction, compounds **1** and **2** are isomorphous and crystallize in the centrosymmetric orthorhombic space group *Pbcn* with an asymmetric unit consisting of one divalent metal ion, one glu dianion and one ligated dpa molecule (Fig. 1, shown for **1**). The metal atoms display a distorted square pyramidal [MN_2O_3] coordination geometry ($\tau=0.223$ for **1**, 0.224 for **2**) [24] with *trans* nitrogen donors from two different dpa ligands anchoring the basal plane. A glu dianion in a 1,5-chelating binding mode fulfills the apical coordination site and one position in the basal plane. The glu ligands in these complexes adopt *gauche–gauche* conformations with four C-atom torsion angles of 62.6° and 65.9° for **1** and 62.2° and 65.4° for **2**. The fourth and final basal plane coordination site in each case is occupied by an oxygen atom from a second glu ligand. Bond lengths and angles (Table 1) are consistent with divalent cobalt and nickel in a distorted square pyramidal coordination environment, with subtle differences consistent with well-established ionic radius trends [25].

Adjacent metal ions are conjoined into zigzag 1D [M(glu)]$_n$ chains parallel to the *b* crystal direction (Fig. 2) through bridging glu carboxylate termini in a *syn-anti* binding mode, in which the basal plane of one square pyramidal coordination sphere is linked to the apical position of another. The M···M distances along the chain motifs in **1** and **2** measure 4.294 and 4.264 Å, respectively. Covalent connectivity within the [M(glu)]$_n$ chains is supplemented by semi-ligation [26] on the part of one of the oxygen donor atoms involved in the 1,5-chelating binding mode of the glu ligands. This oxygen donor atom is bound at the apical coordination site of one metal ion, and donates electron density towards the vacant coordination site of another metal ion. Thus, a 1D repeating [M···O–M···O–]$_n$ chain within the larger [M(glu)]$_n$ chain unit can be invoked. The semi-ligating M···O distances in **1** and **2** are 2.432 and 2.417 Å, respectively, causing respective M···O–M angles of 144.4° and 145.2°.

Juxtaposed [M(glu)]$_n$ chains in **1** and **2** are linked into (4,4) rectangular grid ruffled 2D [M(glu)(dpa)]$_n$ layer parallels to the *bc* crystal plane by exobidentate dpa ligands (Fig. 3). The M···M contact distances through the bridging dpa ligands are 11.806 (**1**) and 11.701 Å (**2**), with an inter-ring torsion within the dpa ligands of 28.7° (**1**) and 28.1° (**2**). The [M(glu)(dpa)]$_n$ single layers in **1** and **2** contrast with those in the similar manganese complex [Mn(glu)(4,4′-bpy)]$_n$ [11]. In this latter material, [Mn_2(glu)$_2$]$_n$ double chains, which lack any sort of M–O···M interaction, are linked into a thick 2D slab by the dipyridyl tethers.

Neighboring [M(glu)(dpa)]$_n$ layers are organized into *pseudo* three-dimensional structures by hydrogen bonding donation between the dpa central amine units projecting above and below

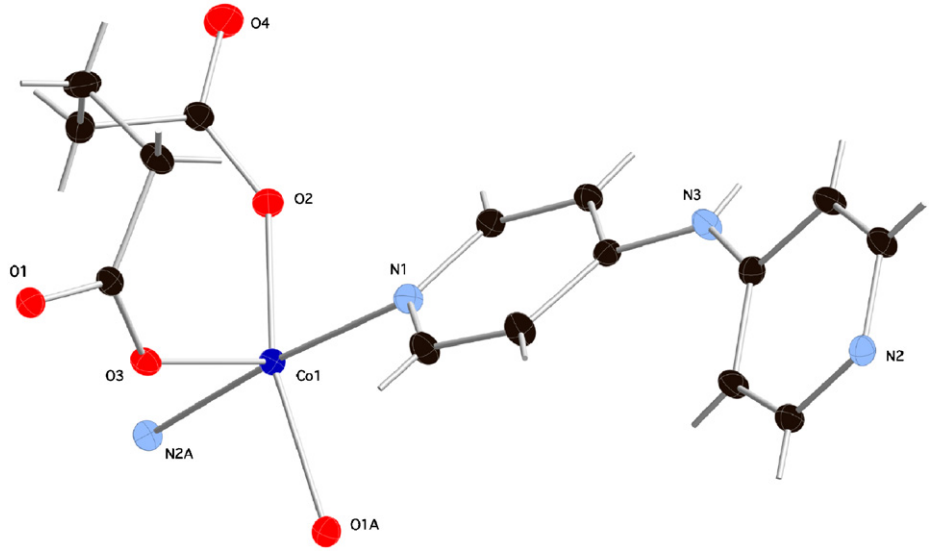

Fig. 1. Coordination environment of **1**. Thermal ellipsoids are shown at 50% probability with partial atom numbering scheme. Hydrogen atoms are represented as sticks. The coordination environment of **2** is very similar.

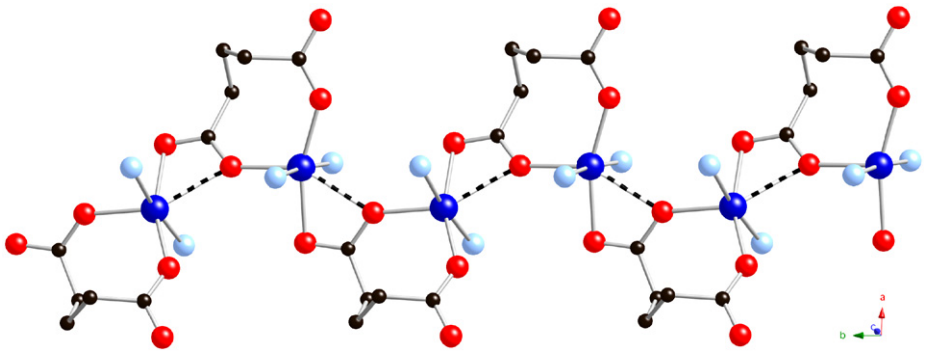

Fig. 2. A $[Co(glu)]_n$ chain in **1**, with semi-ligating interactions shown as dashed lines. The semi-chelating oxygen atom is covalently bound at the apical site of the square pyramidal coordination environment.

each layer, and semi-chelating carboxylate oxygen atoms belonging to glu ligands in two other layers (Fig. S1). To facilitate this supramolecular interaction, the individual layers are arranged in an offset *ABA* stacking pattern. Geometrical parameters for the interlayer hydrogen bonding patterns in **1** and **2** are listed in Table 2. Considering the nitrogen atoms at the dpa ligands' central nitrogen atoms as three-connected nodes, and the metal atoms as five-connected nodes, the overall supramolecular structures of **1** and **2** can be visualized as a (3,5)-connected 3D network with an unprecedented binodal $(4.6^2)(4.6^5.8^4)$ topology (Fig. 4), as analyzed via TOPOS software [27].

4.3. Structural description and single crystal-to-single crystal transformation of $[Cu(glu)(dpa)]_n$ (**3**)

As done for crystals of **1** and **2**, an X-ray diffraction experiment was performed at 173 K on a single crystal of compound **3**. Dissimilar to **1** and **2**, the complex crystallized in the acentric orthorhombic space group $Pca2_1$, with an asymmetric unit consisting of two divalent copper atoms, two glutarate dianions, and two dpa moieties (Figs. 5a and b). Both Cu1 and Cu2 possess distorted square pyramidal $[MN_2O_3]$ coordination geometry ($\tau = 0.273$ and 0.261, respectively) with very similar arrangements and binding modes of glu and dpa ligands to those seen in **1** and **2**. Nevertheless there are subtle variations in bond lengths and angles about the copper atoms (Table 4). Here, the glu dianion bound to Cu1 adopts a *gauche–anti* conformation (torsion angles = 66.1/153.3°), while that bound to Cu2 rests in a *gauche–gauche* conformation (torsion angles = 66.3/62.4°). No crystallographic disorder is evident in the glu ligands in **3** at 173 K; attempts to model the structure in a higher symmetry centrosymmetric space group with one copper atom, one dpa ligand, and one disordered glu ligand failed.

Adjacent Cu1 atoms are linked through the *gauch–anti* conformation glu ligands to form $[Cu(glu)]_n$ 1D chains (*chain-A*, Fig. 6a) with a Cu···Cu distance of 4.694 Å. Similarly, neighboring Cu_2 atoms are conjoined via *gauche–gauche* conformation glu ligands to form crystallographically distinct $[Cu(glu)]_n$ 1D chains (*chain-B*, Fig. 6b) with a Cu···Cu distance over 0.1 Å closer, at 4.589 Å. The varying glu conformations instill different twists of neighboring copper square pyramidal coordination spheres (29° in *chain-A*, 43 ° in *chain-B*). Cu···O semi-ligation within both *chain-A* and *chain-B* provides $[Cu\cdots O–Cu\cdots O–]_n$ chain patterns, with Cu···O distances of 2.778 and 2.600 Å within *chain-A* and *chain-B*, respectively.

Chain-A 1D motifs connect into a 2D $[Cu(glu)(dpa)]_n$ layered motif (*layer-A*) through tethering dpa ligands, with a Cu···Cu

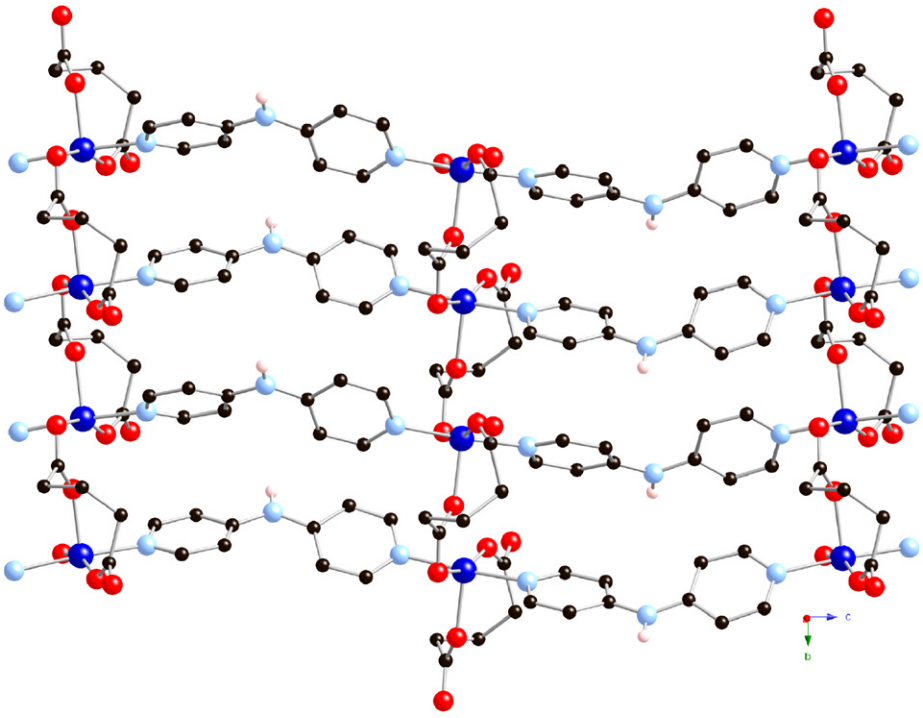

Fig. 3. A single $[Co(glu)(dpa)]_n$ rectangular grid layer in **1**, viewed down the *a* crystal direction.

Table 2
Selected bond distance (Å) and angle (°) data for **1** and **2**

Co1–O2	2.0116(10)	Ni1–O4	2.0049(18)
Co1–O3	2.0760(10)	Ni1–O1	2.0488(17)
Co1–O1$^{\#1}$	2.1101(10)	Ni1–O2$^{\#4}$	2.0711(18)
Co1–N2$^{\#2}$	2.1417(11)	Ni1–N2$^{\#5}$	2.084(2)
Co1–N1	2.1423(11)	Ni1–N1	2.086(2)
O1–C11	1.2570(15)	O1–C11	1.275(3)
O3–C11	1.2750(15)	O2–C11	1.256(3)
O2–C15	1.2698(16)	O3–C15	1.248(3)
O4–C15	1.2404(16)	O4–C15	1.270(3)
O2–Co1–O3	106.86(4)	O4–Ni1–O1	106.43(7)
O2–Co1–O1$^{\#1}$	161.05(4)	O4–Ni1–O2$^{\#4}$	161.35(7)
O3–Co1–O1$^{\#1}$	91.83(3)	O1–Ni1–O2$^{\#4}$	91.89(7)
O2–Co1–N2$^{\#2}$	94.07(4)	O4–Ni1–N2$^{\#5}$	93.92(8)
O3–Co1–N2$^{\#2}$	89.35(4)	O1–Ni1–N2$^{\#5}$	89.00(7)
O1$^{\#1}$–Co1–N2$^{\#2}$	89.11(4)	O2$^{\#4}$–Ni1–N2$^{\#5}$	89.72(8)
O2–Co1–N1	88.28(4)	O4–Ni1–N1	88.33(8)
O3–Co1–N1	94.76(4)	O1–Ni1–N1	94.87(7)
O1$^{\#1}$–Co1–N1	87.07(4)	O2$^{\#4}$–Ni1–N1	86.67(8)
N2$^{\#2}$–Co1–N1	174.47(4)	N2$^{\#5}$–Ni1–N1	174.79(8)

Symmetry transformations to generate equivalent atoms: (#1) −x+3/2, y+1/2, z; (#2) −x+3/2, −y+1/2, z −1/2; (#3) −x+3/2, y−1/2, z; (#4) −x−1/2, y−1/2, z; (#5) −x+1/2, −y+1/2, z+1/2.

through-diimine distance of 11.477 Å. In *layer-A* the inter-ring torsion angle within the dpa ligands subtends 31.1°. In turn, *chain-B* 1D patterns link into similar 2D $[Cu(glu)(dpa)]_n$ units (*layer-B*), with a shorter Cu···Cu through-dpa distance of 11.420 Å fostered by the inter-ring torsion angle of 32.2°. A similar trend, where less acute inter-ring torsion angles result in a shorter through-dpa metal–metal tethering distance, has been observed in other dpa-based aliphatic dicarboxylate coordination polymers [15]. Crystallographically distinct *layer-A* and *layer-B* motifs then stack in an offset alternating pattern via hydrogen bonding mechanisms (Table 3) mediated by the central amine units of the dpa ligands (Fig. 7).

At 293 K, the same crystal of **3** gave single-crystal X-ray diffraction data that could only be acceptably solved in the centrosymmetric orthorhombic space group *Pbcn*. The asymmetric unit consists of one divalent copper ion, one glu dianion and one ligated dpa molecule (Fig. 8). Similar to **1** and **2**, the copper atom displays a distorted square pyramidal $[MN_2O_3]$ coordination geometry ($\tau = 0.26$) with *trans* nitrogen donors from two different dpa ligands anchoring the basal plane. The apical bond length, to a glu carboxylate oxygen atom is elongated by ~0.2 Å due to the Jahn–Teller active d^9 electronic configuration. Bond lengths and angles (Table 4) are consistent with divalent copper in a distorted square pyramidal coordination environment. The flexible glu ligands in **1** are disordered equally over two sets of positions; one set represents a *gauche–gauche* conformation with C–C–C–C torsion angles of 68.0/72.0°, while the other set marks a contrasting *gauche–anti* conformation (64.7/151.1° four-atom torsion angles). The terminal carbon atoms within the glu chain are common to both disordered conformations.

Adjacent copper ions are conjoined into zigzag 1D $[Cu(glu)]_n$ chains virtually identical to those in **1** and **2** by bridging glu carboxylate termini in a *syn–anti* binding mode, in which the basal plane of one square pyramidal coordination sphere is linked to the apical position of another. The Cu···Cu distance along the chain motif in the high temperature form of **3** measures 4.653 Å. Covalent connectivity within the $[Cu(glu)]_n$ chains is supplemented by semi-ligation on the part of one of the oxygen donor atoms involved in the 1,5-chelating binding mode of the glu ligands. This oxygen donor atom is bound at the apical coordination site of one copper ion, and donates electron density towards the vacant coordination site of another copper ion. The semi-ligating Cu···O distance is 2.684 Å, causing a Cu···O–Cu angle of 139.4°.

As in **1** and **2**, dipodal dpa ligands link the $[Cu(glu)]_n$ chains into (4,4) rectangular grid ruffled 2D $[Cu(glu)(dpa)]_n$ layers. The Cu···Cu contact distance through the bridging dpa ligands is 11.472 Å, with an inter-ring torsion within the dpa ligands of 31.7°.

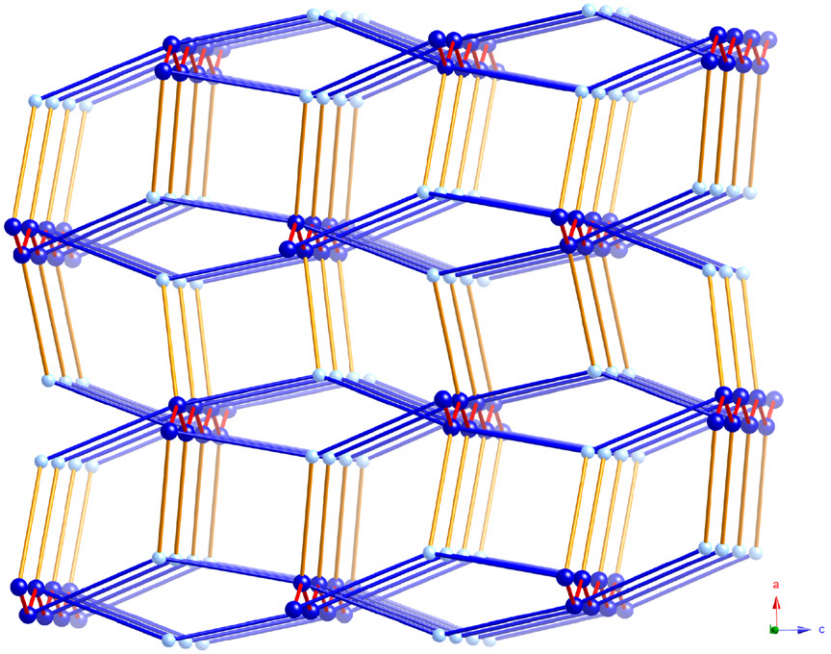

Fig. 4. Schematic perspective of the unprecedented (3,5)-connected supramolecular binodal topology in **1**.

The structure of **3** contrasts markedly with that observed with that of its rigid-rod analog $[Cu_2(glu)_2(4,4'\text{-bpy})]_n$, which contains 2D $[Cu_2(glu)_2]_n$ layers strutted by 4,4′-bpy ligands into a rare 3D *rob* topology [28]. Neighboring crystallographically identical $[Cu(glu)(dpa)]_n$ layers in the high temperature polymorph of **3** are organized into the *pseudo* 3D structure, stacking in an *ABAB* repeat pattern through similar hydrogen bonding patterns as seen in the Co and Ni analogues (Table 3).

Thus, the low temperature and high temperature forms of **3** can be considered polymorphs that can be transformed through a SCSC process. Most SCSC transformations in coordination polymers involve the absorption or desorption of guest molecules [29], and in some rare cases the rearrangement of covalent bonds [30]. The thermally induced SCSC transformation in **3** is not as dramatic, instead more closely mirroring SCSC transformations in organic systems occurring by conformational readjustments [31]. Nevertheless the conformational changes in the flexible glu ligand with coordination polymer **3** provide a mechanism to toggle between acentric and centrosymmetric crystal forms.

4.4. Magnetic properties of *1–3*

Variable temperature magnetic susceptibility measurements were undertaken to investigate the level of spin communication through the $[M\cdots O\text{–}M\cdots O\text{–}]_n$ chain patterns within the $[M(glu)(dpa)]_n$ coordination polymer layers. A plot of the χ_mT product vs T for the nickel derivative **2** reveals a slow descending curve between 300 and ~30 K with a sharper decrease thereafter, potentially indicative of weak antiferromagnetic coupling between neighboring nickel atoms. The data were fit to the expression of Fisher (Eq. (1)) [32] for a 1D Heisenberg chain of coupled spins modified by the inclusion of a temperature independent paramagnetic term (TIP), with $S = 1$ and all other variables having their usual magnetochemical meanings. Best fit parameters for **2** as obtained by non-linear regression were (Fig. 7): $g = 2.117(4)$, $J = -0.28(1)\,cm^{-1}$, and $TIP = 2.9(3)\times10^{-5}$ $cm^3\,mol^{-1}$ with $R = \{\Sigma[(\chi_mT)_{obs}-(\chi_mT)_{calc}]^2\}^{1/2} = 3.3\times10^{-4}$, with the negative sign of the exchange parameter J corroborating the likelihood of intra-chain antiferromagnetic coupling within **2**.

$$\chi_mT = \left[\left(\frac{Ng^2\beta^2S(S+1)}{3k}\right)\left(\frac{1+u}{1-u}\right)\right] + TIP(T) \quad (1)$$

where $u = \coth(2JS(S+1)/kT) - (kT/2JS(S+1))$.

A plot of the χ_mT product vs T for the copper derivative **3** portrays a smooth decline between 300 and 10 K with a precipitous drop at lower temperatures, hinting towards antiferromagnetic coupling between neighboring copper atoms. As for **2**, the variable temperature magnetic data were fit to Eq. (1), but with $S = 1/2$. Best fit parameters for **3** (Fig. 8) were: $g = 2.110(5)$, $J = -0.33(1)\,cm^{-1}$, and $TIP = 1.02(1)\times10^{-3}\,cm^3\,mol^{-1}$ with $R = 1.4\times10^{-4}$. Thus both **2** and **3** appear to exhibit antiferromagnetic superexchange through their respective 1D $[M\cdots O\text{–}M\cdots O\text{–}]_n$ chain motifs.

A plot of the χ_mT product vs T for the cobalt derivative **1** shows a smooth decrease from 300–15 K, below which point it increases to $4.0\,cm^3\,Kmol^{-1}$ at 5.5 K, only to decrease again at low temperatures. Magnetic treatment of d^7 divalent cobalt systems is complicated by both zero-field splitting and unquenched orbital angular momentum. Therefore, the data was fit to a phenomenological expression by Rueff (Eq. (2)) [33], which takes into account both competing single ion effects (D) and magnetic superexchange (J), with C being equivalent to the Curie constant of the material:

$$\chi_mT = A\,\exp(-D/kT) + B\,\exp(J/kT) \quad (2)$$

where $A + B = C = (5Ng^2\beta^2/4k)$.

Fitting the variable temperature susceptibility data to Eq. (2) resulted in best-fit parameters (Fig. 9) of $C = 2.36(3)$ (giving $g = 2.24$), $D = 30(1)\,cm^{-1}$, $J = 14(1)\,cm^{-1}$ with $R = 3.0\times10^{-3}$. Thus, in contrast to the antiferromagnetic tendencies seen in **2** and **3**, the predominant magnetic superexchange pathway is ferromagnetic. This divergent behavior is plausibly ascribed to the overlap of different magnetic orbital sets ("e_g" only in **2** and **3**, both "t_{2g}" and "e_g" in **1**), as reported for other dual-ligand

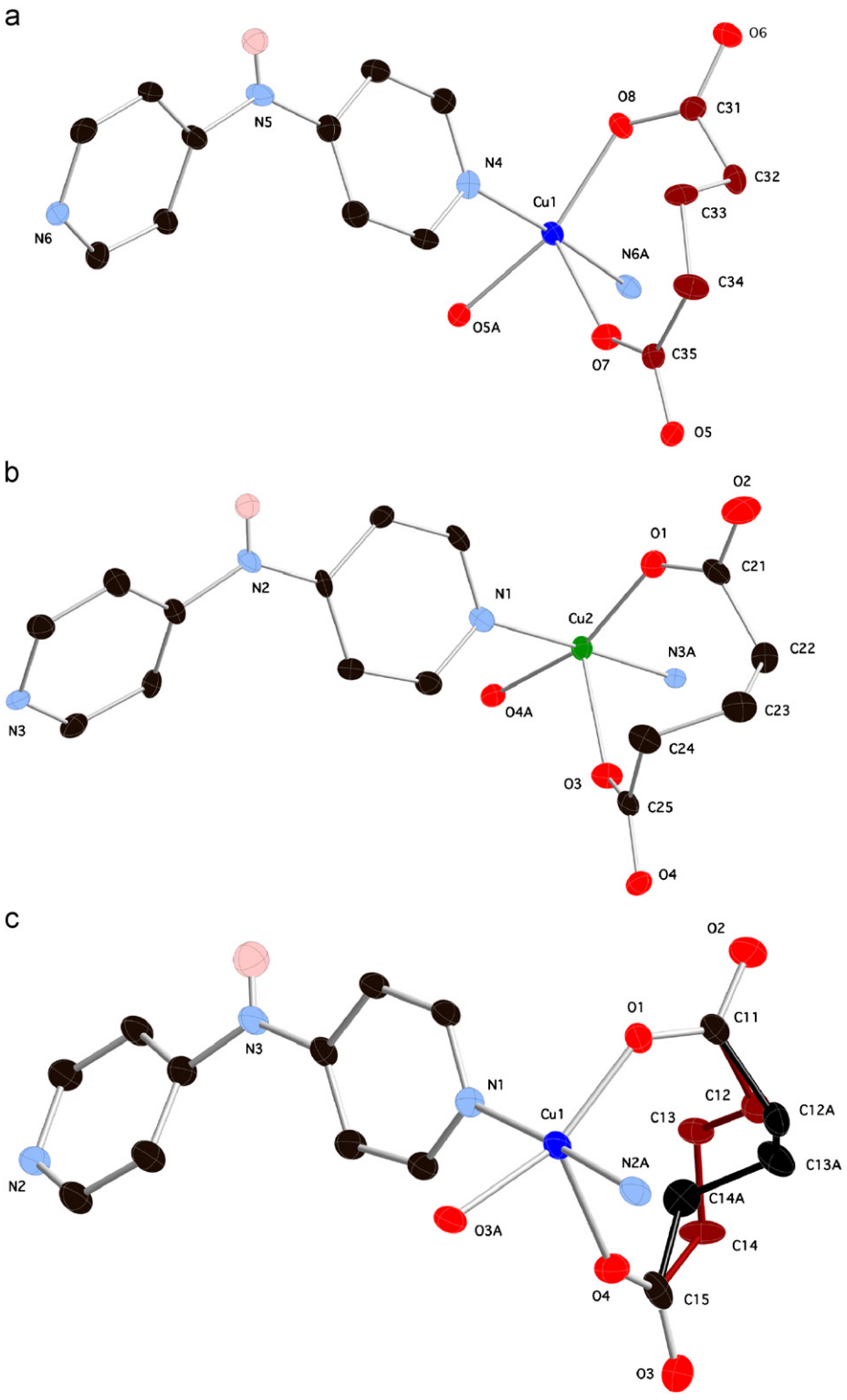

Fig. 5. (a, b) Coordination environments around Cu1 and Cu2 in the low temperature polymorph of **3**. (c) The unique coordination environment in the high temperature polymorph of **3**, showing the two positions of the disordered glutarate ligand. Thermal ellipsoids are shown at 50% probability.

coordination polymer systems [14,34]. An examination of the low temperature magnetic data for **1** (Fig. 10) indicates a sharp decrease in the $\chi_m T$ value below 5.5 K, indicative of either long-range weak antiferromagnetic interaction through the dpa ligands, or more likely, anisotropy-driven spin canting with misalignment of neighboring spins from an idealized ferromagnetic ground state. The data below 5.5 K could not be acceptably fit with Eq. (2).

4.5. Thermogravimetric analysis

All new phases were subjected to thermogravimetric analysis to probe their thermal stabilities. Compound **1** remained stable until ~320 °C, whereupon removal of the organic components occurred. The remaining material at 900 °C, 22.8% of the original mass, corresponds roughly to the deposition of CoO (20.8% calc'd). Compound **2** exhibited no mass loss until ~275 °C, at which point

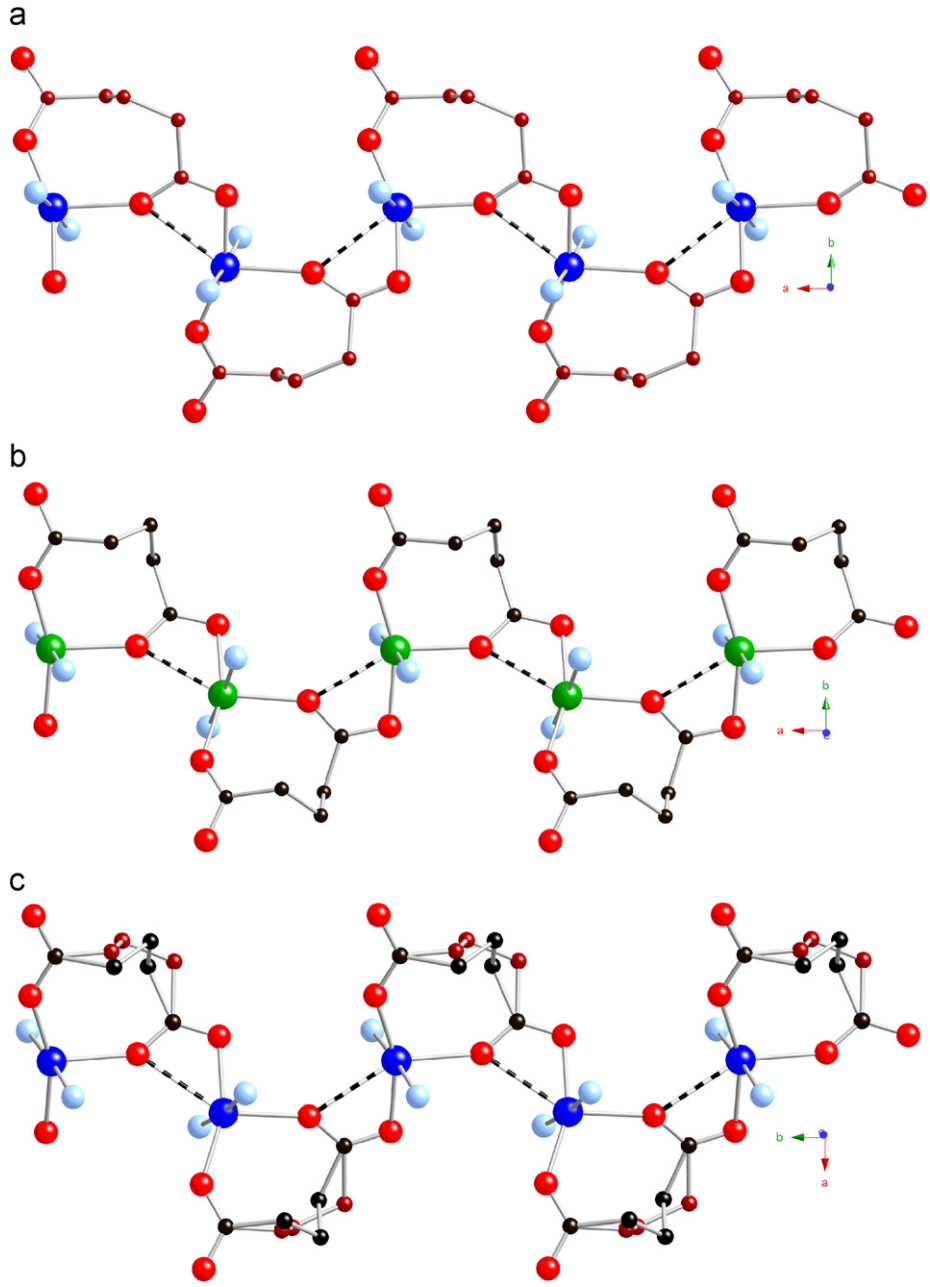

Fig. 6. (a) $[Cu(glu)]_n$ *chain-A* motif in the low temperature polymorph of **3**. (b) $[Cu(glu)]_n$ *chain-B* motif in the low temperature polymorph of **3**. (c) Unique $[Cu(glu)]_n$ chain motif in the low temperature polymorph of **3**. Semi-ligating interactions are shown as dashed lines.

Table 3
Hydrogen bonding distance (Å) and angle (°) data for 1–3

D–H···A	*d*(H···A)	∠DHA	*d*(D···A)	Symmetry transformation for A
1				
N3–H3N···O4	1.926(18)	164.0(16)	2.7290(16)	$-x+2, -y+1, -z+1$
2				
N3–H3N···O3	1.879(19)	162(3)	2.722(3)	$-x+1, -y+1, -z+1$
3 (low temp.)				
N2–H2N···O2	1.934(18)	163(2)	2.755(2)	$x+1, y, z$
N5–H5N···O5	1.929(18)	162(2)	2.735(2)	$x-1, y, z$
3 (high temp.)				
N2–H2N···O2	1.924(17)	164(2)	2.751(3)	$-x+2, -y+1, -z+1$

the organic ligands are expelled. The mass remnant of 31.0% at ~440 °C is consistent with the production of $NiCO_3$ (33.0% calc'd); decarboxylation between ~440 °C and ~700 °C resulted in likely deposition of NiO (20.3% observed remaining mass, 20.8% calc'd). Compound **3** began to expel its organic components at ~250 °C, with a sharp mass loss noted immediately thereafter. A final mass

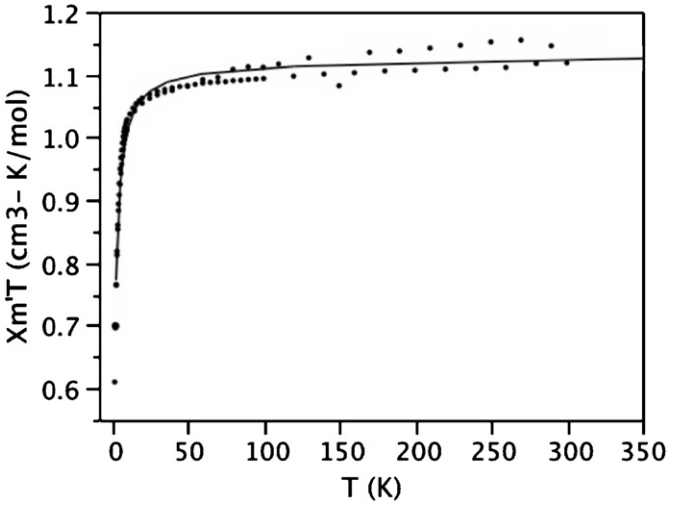

Fig. 7. Plot of $\chi_m T$ vs T for **2**. The solid line represents the best fit to Eq. (1).

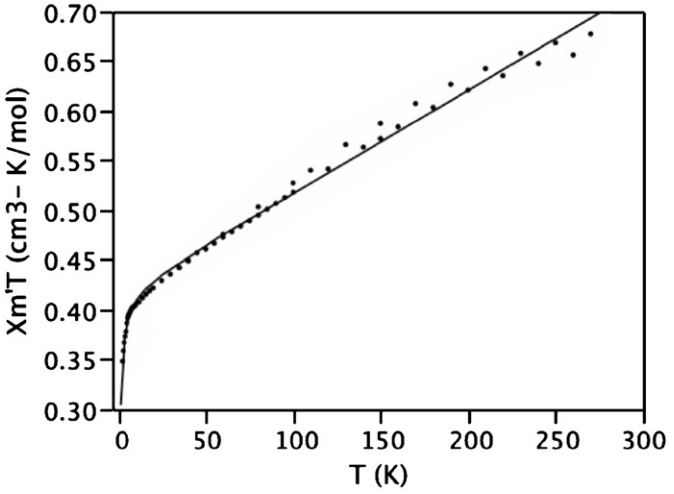

Fig. 8. Plot of $\chi_m T$ vs T for **3**. The solid line represents the best fit to Eq. (1).

remnant of 18.7% of the original is roughly consistent with the deposition of Cu metal (17.4% calc'd). The TGA traces for **1**–**3** are given in Figs. S1–S3.

5. Conclusions

Self-assembly of divalent transition metal cations, glutarate, and the kinked diimine dpa has generated three isostructural coordination polymers wherein neutral 1D $[M(glu)]_n$ chains featuring close M···M contacts fostered by semi-ligation are connected into 2D (4,4) rectangular grid layers. In the case of the copper derivative, low energy conformational changes within the glu ligand, with concomitant adjustment of hydrogen-bonding pathways imparted by the amine functional groups of the dpa moieties, provides access to a single crystal-to-single crystal transformation between centrosymmetric and acentric polymorphs.

The structures of **1**–**3** vary very significantly from their derivatives incorporating either shorter or longer α,ω-dicarboxylate ligands [15–16]. Among these succinate or adipate complexes, only $[Co(adipate)(dpa)]_n$ possesses metal–metal contacts close enough for magnetic communication, within its discrete $\{Co_2\}$ dinuclear units. Thus, the unique conformational capabilities of

Table 4
Selected bond distance (Å) and angle (°) data for **3** (low and high temperature)

3 (low temperature)			
Cu1–O6	1.9642(14)	N1–Cu1–O7	93.78(6)
Cu1–O8$^{\#1}$	1.9788(14)	N3$^{\#2}$–Cu1–O7	87.64(6)
Cu1–N1	2.0250(18)	O1–Cu2–N6$^{\#3}$	95.24(7)
Cu1–N3$^{\#2}$	2.0412(16)	O1–Cu2–N4	88.58(6)
Cu1–O7	2.2918(15)	N6$^{\#3}$–Cu2–N4	175.39(7)
Cu2–O1	1.9680(14)	O1–Cu2–O4$^{\#4}$	160.15(6)
Cu2–N6$^{\#3}$	2.0164(17)	N6$^{\#3}$–Cu2–O4$^{\#4}$	87.91(7)
Cu2–N4	2.0218(18)	N4–Cu2–O4$^{\#4}$	87.63(7)
Cu2–O4$^{\#4}$	2.0246(15)	O1–Cu2–O3	105.15(6)
Cu2–O3	2.2243(14)	N6$^{\#3}$–Cu2–O3	87.92(6)
		N4–Cu2–O3	93.58(6)
O6–Cu1–O8$^{\#1}$	159.35(6)	O4$^{\#4}$–Cu2–O3	94.53(5)
O6–Cu1–N1	90.18(6)	N1–Cu1–N3$^{\#2}$	175.35(7)
O8$^{\#1}$–Cu1–N1	87.20(7)	O6–Cu1–O7	111.22(5)
O6–Cu1–N3$^{\#2}$	93.44(6)	O8$^{\#1}$–Cu1–O7	89.40(5)
O8$^{\#1}$–Cu1–N3$^{\#2}$	88.39(6)		
3 (high temp.)			
Cu1–O1	1.9629(13)	O1–Cu1–N3$^{\#6}$	94.29(6)
Cu1–O3$^{\#5}$	1.9987(15)	O3$^{\#5}$–Cu1–N3$^{\#6}$	88.25(6)
Cu1–N1	2.0261(15)	N1–Cu1–N3$^{\#6}$	175.44(7)
Cu1–N3$^{\#6}$	2.0296(15)	O1–Cu1–O4	107.72(5)
Cu1–O4	2.2715(16)	O3$^{\#5}$–Cu1–O4	92.48(6)
		N1–Cu1–O4	93.57(6)
O1–Cu1–O3$^{\#5}$	159.71(6)	N3$^{\#6}$–Cu1–O4	87.79(7)
O1–Cu1–N1	89.45(6)		
O3$^{\#5}$–Cu1–N1	87.34(6)		

Symmetry transformations to generate equivalent atoms: (#1) x+1/2, −y+2, z; (#2) −x+1, −y+2, z−1/2; (#3) −x, −y+1, z+1/2; (#4) x−1/2, −y+1, z; (#5) −x+3/2, y+1/2, z; (#6) −x+3/2, −y+1/2, z−1/2.

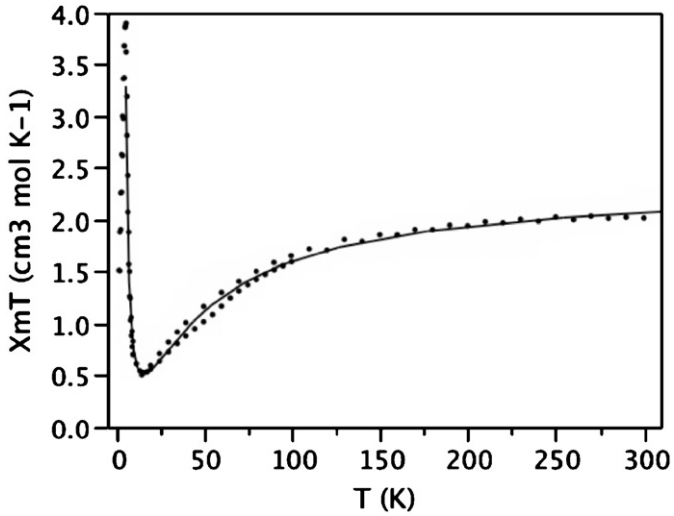

Fig. 9. Plot of $\chi_m T$ vs T for **1**. The solid line represents the best fit to Eq. (2).

the glutarate ligands, in tandem with the kinked donor disposition and hydrogen-bonding facility of the dpa tethers, results in a family of coordination polymers with 1D $[M\cdots O–M\cdots O–]_n$ chain motifs possessing varying magnetic interactions. The nickel and copper derivatives show weak antiferromagnetic coupling along the chain motifs; the variable temperature magnetic behavior in both cases could be interpreted successfully using a classic model. On the other hand, the cobalt analog exhibits competing ferromagnetic ordering and zero-field effects, which results in possible spin-canting behavior at low temperature. Further work towards the synthesis of coordination polymers incorporating substituted or unsubstituted α,ω-dicarboxylate ligands and tethering, hydrogen-bonding capable organodiimines

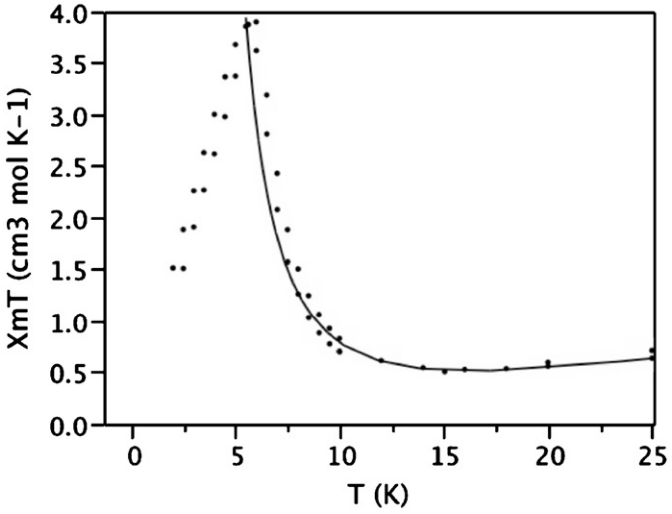

Fig. 10. Low temperature regime plot of $\chi_m T$ vs T for **1**.

is certain to afford materials with novel topologies and intriguing physicochemical properties.

6. Supplementary material

Low temperature crystallographic data (excluding structure factors) for **1** and **2** have been deposited with the Cambridge Crystallographic Data Centre with Nos. 677975 and 677976. The crystal structure data for **3** have CCDC Nos. 679062 (low temperature) and 677977 (high temperature). Copies of the data can be obtained free of charge via the Internet at 〈http://www.ccdc.cam.ac.uk/conts/retrieving.html〉 or by post at CCDC, 12 Union Road, Cambridge CB2 1EZ, UK (Fax: 44–1223336033, Email: deposit@ccdc.cam.ac.uk).

Acknowledgments

The authors gratefully acknowledge Michigan State University for financial support of this work. We thank Dr. Rui Huang (MSU) for elemental analysis (SDG).

Appendix A. Supplementary material

Supplementary data associated with this article can be found in the online version at 10.1016/j.jssc.2008.09.020.

References

[1] J.L.C. Roswell, O.M. Yaghi, Angew. Chem. Int. Ed. Engl. 44 (2005) 4670;
M. Kondo, T. Okubo, A. Asami, S.-I. Noro, T. Yoshitomi, S. Kitagawa, T. Ishii, H. Matsuzaka, Angew. Chem. Int. Ed. Engl. 38 (1999) 140;
A.C. Sudik, A.R. Millward, N.W. Ockwig, A.P. Cote, J. Kim, O.M. Yaghi, J. Am. Chem. Soc. 127 (2005) 7110.

[2] J.S. Seo, D. Whang, H. Lee, S.I. Jun, J. Oh, Y.J. Jeon, K. Kim, Nature 404 (2000) 982;
A. Cingolani, S. Galli, N. Masciocchi, L. Pandolfo, C. Pettinari, A. Sironi, J. Am. Chem. Soc. 127 (2005) 6144.

[3] Q.-R. Fang, G.-S. Zhu, M. Xue, J.-Y. Sun, S.-L. Qiu, Shi-Lun, Dalton Trans. (2006) 2399;
X.-M. Zhang, M.-L. Tong, H.K. Lee, X.-M. Chen, J. Solid State Chem. (2001) 118;
O.M. Yaghi, H. Li, T.L. Groy, Inorg. Chem. 36 (1997) 4292.

[4] S.G. Baca, M.T. Reetz, R. Goddard, I.G. Filippova, Y.A. Simonov, M. Gdaniec, N. Gerbeleu, Polyhedron 25 (2006) 1215;
H. Han, S. Zhang, H. Hou, Y. Fan, Y. Zhu, Eur. J. Inorg. Chem. (2006) 1594;
W. Mori, S. Takamizawa, C.N. Kato, T. Ohmura, T. Sato, Microporous Mesoporous Mater. 73 (2004) 15.

[5] S. Zang, Y. Su, Y. Li, Z. Ni, Q. Meng, Inorg. Chem. 45 (2006) 174;
L. Wang, M. Yang, G. Li, Z. Shi, S. Feng, Inorg. Chem. 45 (2006) 2474;
S. Wang, Y. Hou, E. Wang, Y. Li, L. Xu, J. Peng, S. Liu, C. Hu, New J. Chem. 27 (2003) 1144.

[6] J. Tao, J.X. Shi, M.L. Tong, X.X. Zhang, X.M. Chen, Inorg. Chem. 40 (2001) 6328;
J. Tao, M.L. Tong, J.X. Shi, X.M. Chen, S.W. Ng, Chem. Commun. (2000) 2043;
J.C. Dai, X.T. Wu, Z.Y. Fu, C.P. Cui, S.M. Hu, W.X. Du, L.M. Wu, H.H. Zhang, R.Q. Sun, Inorg. Chem. 41 (2002) 1391;
W. Chen, J.Y. Wang, C. Chen, Q. Yue, H.M. Yuan, J.S. Chen, S.N. Wang, Inorg. Chem. 42 (2003) 944;
N. Hao, E. Shen, Y.B. Li, E.B. Wang, C.W. Hu, L. Xu, Eur. J. Inorg. Chem. (2004) 4102.

[7] W.-G. Lu, C.-Y. Su, T.-B. Lu, L. Jiang, J.-M. Chen, J. Am. Chem. Soc. 128 (2006) 34–35;
S. Horike, R. Matsuda, S. Kitagawa, Stud. Surf. Sci. Catal. 156 (2005) 725–732;
C. Qin, X.-L. Wang, Y.-G. Li, E.-B. Wang, Z.-M. Su, L. Xu, R. Clerac, Dalton Trans. (2005) 2609–2614;
Y.-Q. Zheng, E.-R. Ying, Polyhedron 24 (2005) 397–406;
S.K. Ghosh, J. Ribas, P.K. Bharadwaj, Cryst. Growth Des. 5 (2005) 623–629;
X.-Z. Sun, Y.-F. Sun, B.-H. Ye, X.-M. Chen, Inorg. Chem. Commun. 6 (2003) 1412.

[8] L. Xu, G.-C. Guo, B. Liu, M.-S. Wang, J.-S. Huang, Inorg. Chem. Commun. 7 (2004) 1145.

[9] B. Chen, C. Liang, J. Yang, D.S. Contreras, Y.L. Clancy, E.B. Lobkovsky, O.M. Yaghi, S. Dai, Angew. Chem. Int. Ed. 45 (2006) 1390.

[10] L.-S. Long, Y.-R. Wu, R.-B. Huang, L.-S. Zheng, Inorg. Chem. 43 (2004) 3798–3800.

[11] Y.-Q. Zheng, J.-L. Lin, Z.-P. Kong, Inorg. Chem. 43 (2004) 2590.

[12] P.S. Mukherjee, S. Konar, E. Zangrando, T. Mallah, J. Ribas, N.R. Chaudhuri, Inorg. Chem. 42 (2003) 2695.

[13] L. Pan, H. Liu, X. Lei, X. Huang, D.H. Olson, N.J. Turro, J. Li, Angew. Chem. Int. Ed. 42 (2003) 542.

[14] F.S. Delgado, M. Hernandez-Molina, J. Sanchiz, C. Ruiz-Perez, Y. Rodriguez-Martin, J. Lopez, F. Lloret, M. Julve, CrystEngComm 6 (2004) 106.

[15] M.R. Montney, S. Mallika Krishnan, N.M. Patel, R.M. Supkowksi, R.L. LaDuca, Cryst. Growth Des 7 (2007) 1145.

[16] M.R. Montney, S. Mallika Krishnan, N.M. Patel, R.M. Supkowksi, R.L. LaDuca, Inorg. Chem. 46 (2007) 7362.

[17] D.P. Martin, R.M. Supkowksi, R.L. LaDuca, Inorg. Chem. 46 (2007) 7917.

[18] P.J. Zapf, R.L. LaDuca, R.S. Rarig, K.M. Johnson, J. Zubieta, Inorg. Chem. 37 (1998) 3411–3414.

[19] O. Khan, Molecular Magnetism, VCH Publishers, New York, 1993.

[20] SAINT, Software for Data Extraction and Reduction, Version 6.02, Bruker AXS, Inc., Madison, WI, 2002.

[21] SADABS, Software for Empirical Absorption Correction, Version 2.03, Bruker AXS, Inc., Madison, WI, 2002.

[22] G.M. Sheldrick, SHELXTL, Program for Crystal Structure Refinement, University of Gottingen, Gottingen, Germany, 1997.

[23] M. Kurmoo, C. Estournes, Y. Oka, H. Kumagai, K. Inoue, Inorg. Chem. 44 (2005) 217.

[24] A.W. Addison, T.N.J. Rao, J. Chem. Soc., Dalton Trans. (1984) 1349.

[25] R.D. Shannon, Acta Cryst. A 32 (1976) 751.

[26] J.W. Steed, D.A. Tocher, Polyhedron 13 (1994) 167.

[27] V.A. Blatov, A.P. Shevchenko, V.N. Serezhkin, J. Appl. Crystallogr. 33 (2000) 1193.

[28] B. Rather, M.J. Zaworotko, Chem. Commun. (2003) 830.

[29] M. Kondo, Y. Irie, Y. Shimizu, M. Miyazawa, H. Kawaguchi, A. Nakamura, T. Naito, K. Maeda, F. Uchida, Inorg. Chem. 43 (2004) 6139;
T.K. Maji, K. Uemura, H.C. Chang, R. Matsuda, S. Kitagawa, Angew. Chem. Int. Ed. 33 (2004) 3269;
M. Kurmoo, H. Kumagai, K.W. Chapman, C.J. Kepert, Chem. Commun. (2005) 3012;
M.H. Zeng, X.L. Feng, X.M. Chen, Dalton Trans. (2004) 2217;
D.V. Soldatov, G.D. Enright, J.A. Ripmeester, Chem. Mater. 14 (2002) 348.

[30] J.P. Zhang, Y.Y. Lin, W.X. Zhang, X.M. Chen, J. Am. Chem. Soc. 127 (2005) 14162;
K. Cheng, B.M. Foxman, J. Am. Chem. Soc. 99 (1977) 8102;
O.-S. Jung, S.H. Park, K.M. Kim, H.G. Jang, Inorg. Chem. 37 (1998) 5781;
Q. Chu, D.C. Swenson, L.R. MacGillivray, Angew. Chem. Int. Ed. 44 (2005) 3569;
K. Cheng, B.M. Foxman, J. Am. Chem. Soc. 99 (1977) 8102.

[31] G.R. Desiraju, I.C. Paul, D.Y. Curtin, J. Am. Chem. Soc. 99 (1977) 1594.

[32] M.E. Fisher, Am. J. Phys. 32 (1964) 343.

[33] J.M. Rueff, N. Masciocchi, P. Rabu, A. Sironi, A. Skoulios, Chem. Eur. J. 8 (2002) 1813.

[34] L.-M. Duan, F.-T. Xie, X.-Y. Chen, Y. Chen, Y.-K. Lu, P. Cheng, J.-Q. Xu, Cryst. Growth Des. 6 (2006) 1101.